

# CONJOINT USE OF CODED-APERTURE COLLIMATORS AND MLEM ALGORITHM: TOWARDS LARGE BLOOD VESSELS RECONSTRUCTION AT 511 KEV

Xavier Hubert<sup>1</sup>, Dominique Chambellan<sup>1</sup>, Samuel Legoupil<sup>1</sup>, Jean-Robert Deverre<sup>2</sup>, Nikos Paragios<sup>3,4</sup>

<sup>1</sup>CEA/DRT/DeTeCS/SSTM/LID, Paris

<sup>2</sup>CEA/DSV/I2BM, Orsay

<sup>3</sup>Laboratoire Mathématiques Appliquées aux Systèmes, Ecole Centrale de Paris

<sup>4</sup>Equipe GALEN, INRIA Saclay, Ile-de-France

## ABSTRACT

In this paper, we propose a novel approach to improve the trade-off between the spatial resolution and the sensitivity of existing nuclear imaging systems in emission tomography for 511 keV-photons. Although emission tomography suffers from the low amount of emitted photons in the object, partial transparency of collimators and low sensitivity of detectors, we are able to reconstruct radioactive spatial distribution from projections obtained through a specifically designed coded-aperture collimator, with a MLEM-algorithm.

We address both the selection of the collimator and the reconstruction approach. Very promising experiments towards 3D-vessels reconstruction demonstrate the potentials of our approach.

**Index Terms**— Nuclear medical imaging, emission tomography, coded-aperture imaging, near-field domain, statistical reconstruction algorithm

## 1. INTRODUCTION

Nuclear imaging offers the opportunity to obtain functional information in a non-invasive way. Common methods for functional imaging rely on Positron Emission Tomography (PET), which allows mapping cerebral deposition of radiotracers along time. In this context, the concentration of radiotracers in blood which enters in the brain is of capital importance since it enables to perform compartmental analysis [1]. The evolution of the radiotracers in blood is called the  $\beta^+$ -input function and is usually measured through arterial blood sampling [2]. This method is invasive and painful for patients. Moreover medical personal are exposed to radiation and potential contamination through manipulation of radioactive blood samples. Lots of efforts have been devoted to perform non-invasive measurement of  $\beta^+$ -input function. Several techniques have been investigated. Some rely on its extraction straight from the 3D-reconstruction of arteries in

the brain [3], but quantification problems arise due to partial volume effect. Furthermore, it is difficult to extract a small structure with low activity from large volume with higher activities. Indeed, radio-labelled molecules are designed so that part of them are stopped in the brain, whereas arteries are just a transportation mean. Some external detectors have also been developed [4], but the spatial resolution does not allow to assess the volume of a section of the artery.

An alternative is to externally measure the activity evolution in arteries along time. The  $\beta^+$ -input function estimation requires both the determination of activity in a section of an artery and its volume. This paper addresses exclusively the volume estimation part of the problem. This is a challenging task since it requires to design an imaging system and its corresponding reconstruction algorithm which offer both good spatial resolution and good sensitivity at 511 keV. Reconstruction and quantification in emission tomography suffer from low signal-to-noise ratio due to the low amount of emitted photons in the object, partial transparency of collimators and low sensitivity of detectors.

Our method is based on the measurement of activity in blood vessels with external detectors. We do not take advantage of coincidences, but instead we acquire images and reconstruct 3D spatial distribution with collimated imaging system. As a result, besides  $\beta^+$ -input function estimation, it is also adapted to perform SPECT on small volumes that emits a low amount of photons.

## 2. METHODS AND MATERIALS

Main problem is the low number of emitted photons along clinical acquisitions. Imaging system must be very sensitive and have a good spatial resolution in order to be able to spatially separate artery from vein, which always stand one next to the other. The measurement location has to offer a good trade-off between the depth of the artery in the body, its diameter and the amount of surrounding noise. As a result we have chosen to simulate configurations which model popliteal artery and vein at the knee location. At this point, vessels

We thank staff of LIME laboratory from Service Hospitalier Frederic Joliot, Orsay, France

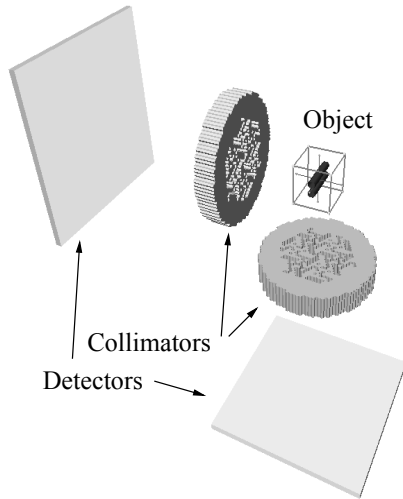


**Fig. 1.** Configuration of the imaging system, based on two HURA collimators and two planar detectors

stand around 50 mm-deep from the surface of the skin and their diameter is 5 mm-large. Furthermore it stands far away from active organs as brain, heart and bladder and it is possible to add extra-collimation in order to reduce the contributions of other sources than vessels. Along clinical acquisitions, average radiotracer concentration in arteries is usually about 1 %ID/100ml [5], where ID denotes the injected dose. The maximum injected dose is 370 MBq for clinical purposes. As a result, average concentration during clinical acquisitions is about  $4 \text{ Bq}\cdot\text{mm}^{-3}$  in every vessel. For a vessel which has a 20 mm-long section in the field of view of the camera and whose diameter is 5mm-large,  $6.6 \times 10^6$  photons are emitted along a 90 min clinical acquisition for  $^{18}\text{F}$ .

A collimated imaging system has been designed to reconstruct volume of both artery and vein. For our method, coincidences are not used because it would require many detectors which would result in an expensive solution. Traditional collimators in Single Photon Emission Computed Tomography (SPECT) have a poor spatial resolution at 511 keV and SPECT is never used for high spatial resolution imaging at such energy. A way to improve efficiency without significantly deteriorating resolution is to use coded-aperture collimators [6]. More than half of incident photons go through collimator, which has to be compared to just a few percents with other collimators. Collimators need to be several millimetre-thick to be able to collimate 511 keV-photons [7]. Contrary to normal reconstruction methods with coded apertures, we have investigated performances of a MLEM-algorithm on such an imaging system. The reason is that correlation product which usually reconstructs the spatial distribution can not deal with 3D-object with collimators whose thickness is not negligible compared to the dimension of holes. Conjoint use of coded-aperture collimators and MLEM algorithm is well adapted to

emission tomography with low amount of emitted photons from objects. Indeed coded apertures have an excellent geometrical efficiency and MLEM algorithm takes into account Poisson nature of the number of detected photons in every pixel of the detector.

The configurations of simulations and experiments are presented on figure (1). Collimators are made of tungsten and they are 9 mm-thick. They belong to HURA-family [8]. Their rank is 6 and the step between centres of holes is 1.85 mm on a hexagonal grid. Distance between the centre of object and collimator centres is 50 mm. Distance between collimators and detectors is 100 mm. We modelled and used a  $\gamma$ -camera ( $\gamma$ -imager S/CT, Biospace, Paris). Detectors are made of CsI-scintillator which is 4 mm-thick. Detector is 100 mm-large and produces 1111x1111-pixel images, that are reorganised as 128x128-pixel images because of computational considerations. With Monte-Carlo simulations, we have estimated that the number of detected photons per projection is 12000 when  $6.6 \times 10^6$  photons are emitted from one cylinder, as calculated previously in this section. As we want to discriminate artery from vein, two cylinders must be placed in the field of view. The count limit in every projection is then 24000; final objective is consequently to be able to reconstruct spatial distribution with projections being under this limit.

First we have evaluated this imaging system with analytically generated data, then from Monte Carlo-generated data using GATE [9] and finally we performed real data acquisitions. This paper only presents results obtained from real data acquisitions. As only one camera is for the moment at our disposal, the two orthogonal projections were acquired separately, by turning the object with a  $90^\circ$ -angle along the line-source axis.

Because of considerations on available equipments, we made a few modifications to the experimental set-up. Indeed, the  $\gamma$ -camera that we can dispose of is electronically

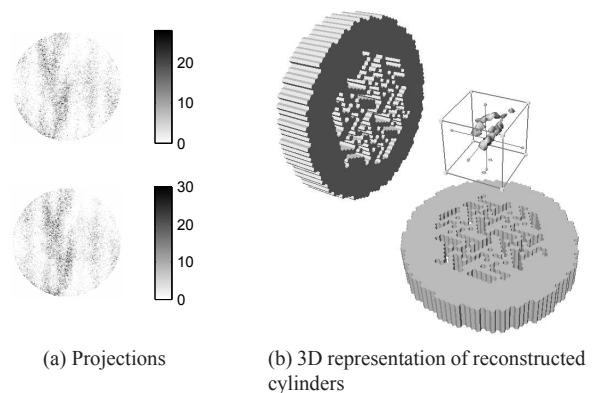


**Fig. 2.** (2a) Projections of two line-sources on detectors. (2b) 3D-representation of the reconstructed spatial distribution of both cylinders

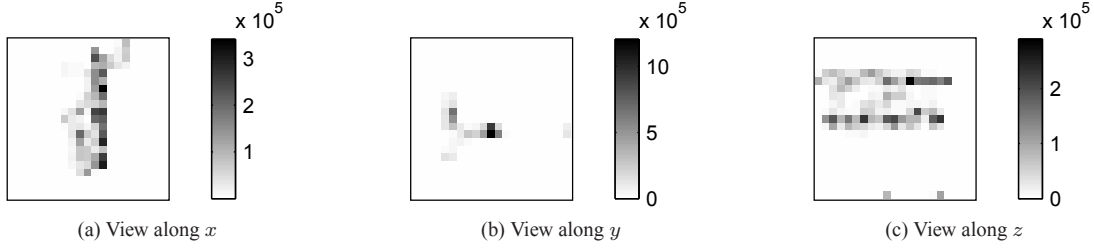


**Fig. 3.** Integrated activity of raw data in x-,y- and z-directions

calibrated so that its sensitivity is null above 350 keV. As we want to understand ML-EM reconstruction behaviour associated with coded-aperture collimators at 511 keV, we built another HURA mask made of a Zn-Sn alloy (75%/25%). The point is that the linear attenuation coefficient of this alloy at 122 keV is equal to tungsten linear attenuation coefficient at 511 keV:  $\mu_W(511 \text{ keV}) = \mu_{Zn,Sn}(122 \text{ keV}) = 2.57 \text{ cm}^{-1}$ . Transparency conditions are then similar. Then, we worked with point-source  $^{57}\text{Co}$  which mainly emits photons whose energy is 122 keV and simulates properly  $^{99}\text{Tc}$ . We used  $^{57}\text{Co}$  instead of  $^{99}\text{Tc}$  because it is more convenient to use a sealed point-source. This point-source has been linearly moved in the field of view during acquisitions in order to model a line-source. The range of the linear displacement is 18 mm. Point-source is a sphere whose diameter is 1 mm-large. Point-source activity is 820 kBq and acquisition lasts 40 seconds.

In emission tomography, radioactive spatial distribution is denoted  $\lambda$ , images are denoted  $Y$  and the direct model which links  $\lambda$  to  $Y$  is denoted  $A$ :  $Y = A\lambda$ . With these standard notations, likelihood function is:

$$L(\lambda) \propto P(Y|\lambda) = \prod_i \frac{(A\lambda)_i^{Y_i} e^{-(A\lambda)_i}}{Y_i!}$$

This requires to have a direct model  $A$  of the projection of the object  $\lambda$  on detectors  $Y$ . We calculate it with a raytracing algorithm. Every coefficient  $a_{i,j}$  of  $A$  is the probability that a photon which is emitted from voxel  $j$  is detected in pixel  $i$ . Iterative estimations  $\hat{\lambda}$  of the most likely spatial distribution of the object are then calculated according to MLEM algorithm [10]:

$$\forall j, \hat{\lambda}_j^{k+1} = \frac{\hat{\lambda}_j^{k+1}}{\sum_i a_{i,j}} \cdot \sum_i \frac{a_{i,j} Y_i}{\sum_k a_{i,k} \hat{\lambda}_k^n}$$

where  $\hat{\lambda}_j^k$  is the activity estimate of voxel  $j$  at iteration  $k$ .

### 3. RESULTS

We acquired projection data sets for various line positions. For each position, we made a first acquisition, and then a second after rotating the object by  $90^\circ$  along cylinder axis. For the experiment of figure (2), we added projections of two line-sources whose centre-to-centre distance is 5 mm. Number of

detected photons are respectively 49374 and 46151 in figure (2a). These two projections allow to reconstruct spatial distribution that is shown on figure (2b). Spatial distribution is reconstructed on a  $(21 \times 21 \times 21)$ -grid, with every voxel volume being  $(1 \times 1 \times 1) \text{ mm}^3$ . This figure shows isosurface on reconstructed voxel activities. Two cylindrical distributions are visible. It is possible to reconstruct 3D spatial distribution from just two projections because coded-aperture collimators allow photons to go through, although they have a direction far from the normal of the collimator. Figure (3) represents integrated observations along x-, y- and z-directions. In section 2, it is mentioned that the range of the linear displacement is 18 mm, which is confirmed in figures (3a) and (3c) since these images are 21 mm-large. Although cylindrical distributions are clearly observable on this figure, reconstruction suffers from inhomogeneities. It has to be mentioned that reconstruction has not been regularised by any spatial *prior*. It has been arbitrarily chosen that the algorithm stops when log-logarithm is not improved more than a factor of 1,1 between two successive iterations, that is to say when  $\ln(L^{k+1}) - \ln(L^k) < 1, 1$ . Inhomogeneities would be reduced through the regularisation of the reconstruction with spatial *prior*, as Gibbs or quadratic *priors*.

Centre-to-centre distances in every slice along the cylinder axis have been calculated. The mean distance is 5.6 mm with a standard deviation which is equal to 1 mm. A bias appears, since the mean distance should have been 5 mm, but reconstructed mean distance is close from real centre-to-centre distance. This means that the spatial resolution is good enough to separate the two cylinders. However number of detected photons is twice too large.

We made ten times identical experiments. Only differences between projections are due to Poisson noise. By adding projections, we can reconstruct projections with various amount of detected photons in it. As the reference object is not exactly known, the root mean square has been calculated in the following way:

- Reconstruction has been performed on the ten acquisitions which have been summed together, for both projections. Reconstructed object is denoted  $\hat{\lambda}_{ref}$ . We normalise  $\hat{\lambda}_{ref}$  so that data becomes comparable:  $\hat{\lambda}_{ref}$  is divided by  $\sum_i (A\hat{\lambda}_{ref})_i$ .
- Reconstructions have been performed multiple times

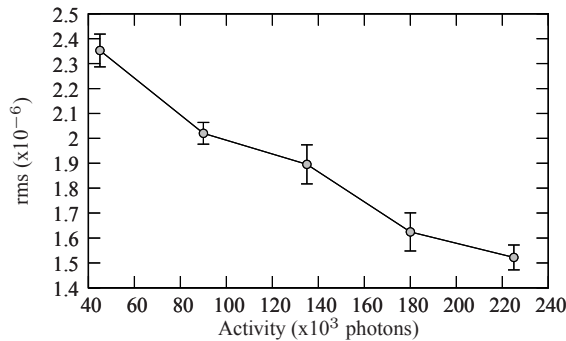


Fig. 4. Statistical rms vs activity

on linear independent combinations of every projection. Before calculating the root mean square, reconstructed spatial distribution has been normalised by dividing  $\hat{\lambda}$  by  $\sum_i (A\hat{\lambda})_i$ .  $rms$  has then been calculated as:

$$rms = \frac{1}{N} \sqrt{\sum_i (\hat{\lambda}_{ref} - \hat{\lambda})_i^2}$$

Figure (4) presents the trend that root mean square follows as amount of detected photons increases. As expected, reconstructions are more accurate when the number of detected photons increases.

#### 4. CONCLUSION AND DISCUSSION

ZnSn alloy allows having similar transparency conditions at 122 keV that tungsten at 511 keV. Although this method is very efficient to evaluate the impact of the collimator in the reconstruction process, it is not able to draw definitive conclusions on results. Indeed, this method compensates for the efficiency of the detector at 511 keV from 122 keV-experiments, but spatial resolution of the detector is better at 122 keV than at 511 keV and incidences of the degradation of the spatial resolution is difficult to assess in term of reconstruction quality.

Our method is able to deal with problems with low amount of emitted photons at high energy. In such conditions, coded aperture collimators and MLEM algorithm are complementary and well-adapted to extract maximum amount of information about the spatial distribution of the activity. These results have to be confirmed by acquisitions with larger cylinders, and then with *in-vivo* experiments on animals and eventually humans.

Another part of the problem is then to process acquired data frame by frame in order to estimate the most likely repartition of activity between volumes of the artery, the vein and the background, so that the  $\beta^+$ -input function can be finally estimated.

#### 5. REFERENCES

- [1] H. Watabe, Y. Ikoma, Y. Kimura, M. Naganawa, and M. Shidahara, "PET Kinetic Analysis-Compartmental Model," *Ann. Nucl. Med.*, vol. 20, no. 9, 2006.
- [2] L. Eriksson, S. Holte, C. Bohm, M. Kesselberg, and B. Hovander, "Automated Blood Sampling Systems for Positron Emission Tomography," *IEEE Trans. on Nucl. Sci.*, vol. 35, Feb. 1988.
- [3] M. Naganawa, Y. Kimura, K. Ishii, K. Oda, K. Ishiwata, and A. Matani, "Extraction of a Plasma Time-Activity Curve from Dynamic Brain PET Images based on Independent Component Analysis," *IEEE Trans. Biomed. Eng.*, vol. 51, 2005.
- [4] A. Kriplani, D.J. Schlyer, P. Vaska, S.P. Stoll, S.J. Park S. Southekal, C.L. Woody, S. Junnarkar, and J.F. Pratte, "Non-invasive and Selective Measurement of the Arterial Input Function using a PET Wrist Scanner," in *Nuclear Science Symposium Conference Record*. IEEE, 2006, vol. 6, pp. 3266 – 3270.
- [5] J.D. Gallezot et al., "In Vivo Imaging of Human Cerebral Nicotinic Acetylcholine Receptors with 2-<sup>18</sup>Fluoro-A-85380 and PET," *J. Nucl. Med.*, vol. 46, 2005.
- [6] R. Accorsi, F. Gasparini, and R.C. Lanza, "A Coded Aperture for High-Resolution Nuclear Medicine Planar Imaging with Conventional Anger Camera: Experimental Results," *IEEE Trans. Nucl. Sci.*, vol. 48, no. 6, December 2001.
- [7] Roberto Accorsi, *Design of Near-Field Coded Aperture Cameras for Medical and Industrial Imaging*, Ph.D. thesis, Massachusetts Institute of Technology, Dept. of Nuclear Engineering, 2001.
- [8] M.H. Finger and T.A. Prince, "Hexagonal Uniformly Redundant Arrays for Coded-Aperture Imaging," in *Proc. 19th Int. Cosmic Ray Conf.*, 1985, pp. 295–298.
- [9] I. Buvat and D. Lazaro, "Monte-Carlo Simulations in Emission Tomography with GATE: An Overview," *Nuclear Instruments and Methods in Physics Research A*, vol. 569, no. 2, 2006.
- [10] K. Lange and R. Carson, "EM Reconstruction Algorithms for Emission and Transmission Tomography," *J. Comp. Assist. Tomo.*, vol. 8, pp. 306–316, april 1984.